Disorder scattering in graphene nanoribbons

F. Libisch[1], S. Rotter[1], J. Burgdörfer[1]
[1] *Institute for Theoretical Physics, Vienna University of Technology, Wiedner Hauptstraße 8-10, A-1040 Vienna, Austria, EU*

We investigate transport through bulk-disordered graphene nanoribbons and nanoconstrictions. Employing a modular recursive Green's function algorithm, we study devices of realistic size (up to 100.000 nm^2). By Fourier transforming the scattered wave we disentangle inter-valley scattering between the two Dirac cones of graphene and intra-valley scattering on a single cone. We find that different types of defects leave characteristic signatures on transport properties which we can describe with a simplified scattering model. A quantitative comparison with recent experimental data is performed which yields insights into the disorder concentration in realistic samples.

I. INTRODUCTION

Graphene[1,2], the first true two-dimensional solid, is a promising candidate for novel nanoelectronic devices due to unique features of the band structure near the Fermi energy. The double cone near the K and K' points of the sub-lattices in reciprocal space gives rise to a near "pseudo-spin" degeneracy, resembling the state space of massless Dirac four spinors. Envisioned applications range from high-mobility nanoelectronics[3], spin-qubits in graphene quantum dots[4] and the creation of "neutrino" billiards[5,6]. Spin coherence times in graphene are expected to be very long due to weak spin-orbit and hyperfine couplings[7,8] making graphene quantum dots promising candidates for future spin based quantum computation[4]. However, confining electrons in graphene is a challenge, mainly due to the gapless electronic structure and the Klein tunneling paradox[9–11]. This difficulty has recently been overcome by structuring 2D graphene and quantum mechanical confinement effects have been observed in nanoribbons[12–14], interference devices[15], single electron transistors[16,17] and in graphene quantum billiards[6].

While the consequences of the hexagonal symmetry of the perfect honeycomb lattice are theoretically well understood, realistic graphene samples feature finite-size effects, symmetry-breaking due to point scatterers and charged impurities. The question is posed as to what extent these defects will influence the properties of graphene. For large-scale devices with random impurities or lattice defects analytical techniques are generally not well suited to address this problem. To elucidate the influence of disorder on graphene devices we will thus employ numerical techniques to simulate transport through bulk-disordered graphene nanowires and nanoconstrictions. We consider both the effect of point defects (lattice vacancies) that break the SU(2) symmetry of the graphene lattice and of a smooth random background potential (e.g., through substrate interactions[18]) and identify specific signatures these different disorder scattering processes induce.

(a) Single vacancy (b) Double vacancy

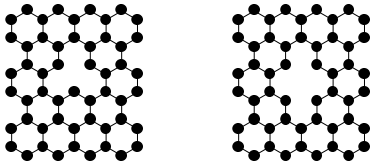

FIG. 1. Prototype defects to simulate (a) sublattice-symmetry breaking scattering at single vacancies and (b) sublattice-symmetry conserving scattering at double vacancies.

II. TECHNIQUE

We employ a tight-binding (TB) approximation to calculate transport properties of graphene nanodevices,

$$H = \sum_{i,s} |\phi_{i,s}\rangle V_i \langle\phi_{i,s}| - \sum_{(i,j),s} \gamma_{i,j} |\phi_{i,s}\rangle \langle\phi_{j,s}| + h.c.\,, \quad (1)$$

where V_i represents the on-site energy of lattice site i induced, e.g., by an electrostatic potential, and $\gamma_{i,j}$ is the tight-binding coupling matrix element between lattice sites i and j. To accurately reproduce the bandstructure of a realistic graphene flake, we include third nearest-neighbor (3NN) coupling[19]. This allows for four free parameters, namely the site-energy ε_0 and the overlap integrals $\gamma_{1,2,3}$, representing the interaction with the first, second and third nearest neighbor. The resulting dispersion relation features a double-cone structure with a linear dispersion relation near $E = 0$ (see envelope of individual transmission modes in Fig. 2). We determine the γ_i by fitting the resulting band structure to ab-initio calculations of the bandstructure, taken from Reich et al.[19]. As the transport properties of graphene are primarily determined by the bandstructure near the Dirac point, we perform the fit within an energy interval of ±2eV around the Fermi energy, giving the parameter set

$$\begin{aligned} \varepsilon_0 &= 0.026\text{eV}, \quad & \gamma_1 &= 3.145\text{eV}, \\ \gamma_2 &= 0.42\text{eV}, \quad & \gamma_3 &= 0.35\text{eV}. \end{aligned} \quad (2)$$

The additional freedom of choosing γ_2 and γ_3 greatly increases the accuracy of the tight-binding description,

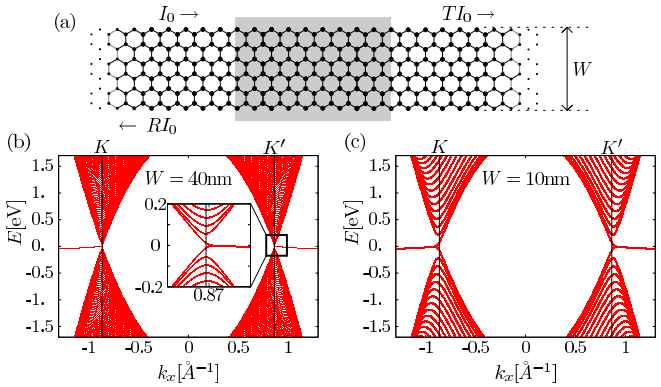

FIG. 2. (a) Scattering geometry investigated in this article: an infinite graphene nanoribbon of width W, with an incoming flux I_0. Inside a finite scattering region (shaded) we place lattice defects and a smooth disorder potential . Due to scattering at the defects the incoming flux is partly reflected (RI_0), the remainder is transmitted (TI_0, $R+T=1$). (b,c) One-dimensional bandstructure of a graphene nanoribbon for two ribbon widths (see insets). For energies farther away from the Dirac points of the K and K' cones, the dispersion relation gets distorted due to trigonal warping.

in particular in energy regions away from the Dirac point. Due to the hexagonal lattice, the double-cone structure of the dispersion relation becomes deformed. Near the K-point this effect commonly referred to as trigonal warping[20] results in a pronounced asymmetry of the Dirac cone (see asymmetry of the bandstructure in Fig. 2). Note that lower-order (i.e. first-order) tight-binding calculations fail to *quantitatively* account for trigonal-warping due to the limited number of free parameters[19].

We consider a graphene nanoribbon of width W [see Fig. 2(a)] with a disordered region of length L. The incoming flux I_0 is partially reflected (with partial flux RI_0) and partially transmitted (with partial flux TI_0). Due to the finite width of the nanoribbon, the transverse component of the wavevector is quantized. As a consequence, the cone-like dispersion relation of the extended system is converted to a discrete set of curves [see Fig. 2(b,c)]. The spacing ΔE in energy between the minima of consecutive curves (e.g., between the onset of new modes) is, approximately, constant and proportional to the wavenumber difference Δk,

$$\Delta E = \hbar v_{\rm F} \Delta k, \quad \text{with} \quad \Delta k \approx \pi/W\,. \tag{3}$$

The spacing between discrete modes (and thus quantization steps) scales inversely with W [compare (b) and (c) in Fig. 2]. The conductance G of an ideal zigzag graphene nanowire features quantization plateaus with a step height of two conductance quanta, $2e^2/h$ (neglecting spin), due to the two degenerate contributions of the K and K' cones.

III. POINT DEFECTS

The first type of disorder we consider are point defects, e.g., scattering potentials with a typical length scale of one unit cell of 2.4 Å, i.e., short-ranged compared to the typical wavelength $\lambda = 2\pi/\delta k$, where δk is the distance (in k-space) to the K point. In the experiment, such defects occur either due to defects in the lattice itself (e.g., lattice vacancies) or chemisorbates that effectively remove single carbon p_z orbitals as available hopping sites for transport. Previous theoretical work on phase-coherent quantum transport has shown that small atomic-scale edge defects can lead to the formation of a transport gap[21] and to Anderson localization[22]. Quantization plateaus in the conductance of graphene nanoribbons have been found to be very sensitive to short-range defects that break the SU(2) symmetry of the AB lattice[23,24]. In particular, single vacancies that break the sublattice symmetry effectively wash out size quantization plateaus, while double vacancies that conserve sublattice symmetry leave them approximately intact (see Fig. 3). This difference results from the strong inter-mode scattering induced by the breaking of sublattice symmetry[24]. Since variations of the local electronic environment of individual carbon atoms by, e.g., substrate interactions, also affect the sublattice symmetry, the experimental observation of size quantization peaks in graphene has remained a challenge which seems to have been overcome only just recently[25]. Double vacancies feature an additional "internal degree of freedom for disorder": the angle of orientation α of the lattice vector connecting the two vacancies relative to the ribbon axis. In our simulations we assume a complete random orientation with equal statistical weight for all three possible orientations (i.e. 30°, 90°, or 150° with respect to the zigzag ribbon axis). Since the angle of orientation has no immediate influence on the persistence of the A-B sublattice symmetry, we expect our results to be, to first order, independent of α. To test this assumption, we have performed calculations with only one of the three possible double vacancy orientations. We find only a slight decrease in reflection R for the $\alpha = 90°$ orientation, with a relative change $\Delta R/R$ compared to $\alpha = 30°$ or $\alpha = 150°$ (which are equivalent) of below 5%.

To visualize the effect of disorder scattering, we calculate the Fourier transform of the incoming (I), reflected (R) or transmitted (T) part of the wavefunction ($i = I, R, T$):

$$\mathcal{F}[\psi_i](k_x) = \int \mathrm{d}y \left| \int \mathrm{d}x\; \psi_i(x,y) e^{ik_x x} \right|^2 \tag{4}$$

The Fourier transform $F[\psi_I]$ of the incoming wave features a pronounced peak at the K point in reciprocal space as the incoming wave only contains a single excited mode (see top row in Fig. 4), located on the K cone. In the reflected and transmitted part, a second peak at K' appears due to $K - K'$ scattering inside the scattering region (see bottom rows in Fig. 4). While both single

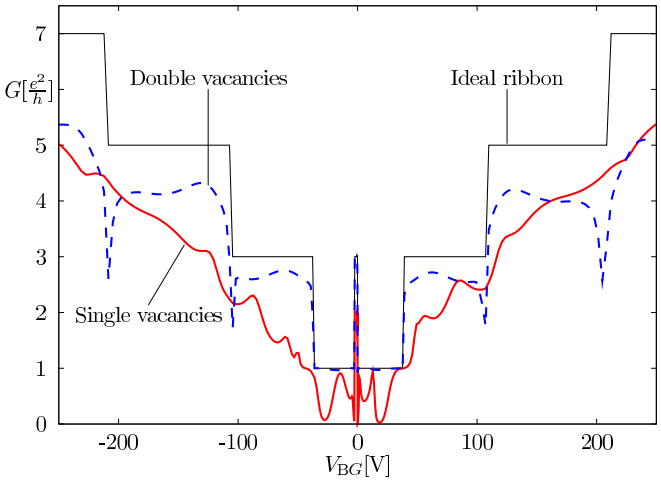

FIG. 3. Conductance of a graphene nanoribbon with width $W = 30nm$ as a function of back-gate voltage V_{BG}. The solid red line (blue dashed line) shows the results for 30 single (double) vacancies in the ribbon. To express the particle energy E as a function of back-gate voltage V_{BG} we used $E = \hbar v_F \sqrt{\eta}$, with effective capacitance $\eta = 7.2 \cdot 10^{14} \mathrm{V}^{-1}\mathrm{m}^{21}$.

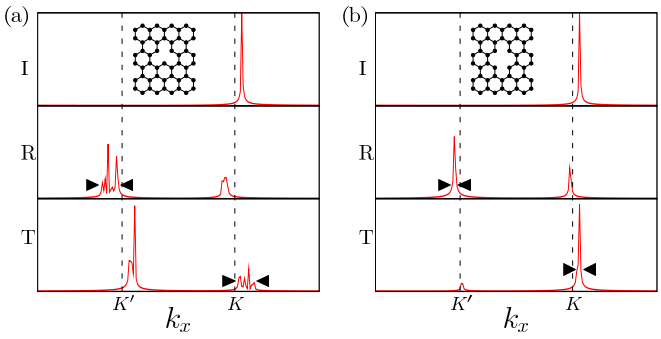

FIG. 4. Fourier transform of scattering through a $W = 15$nm wide zigzag graphene nanoribbon for (a) 10 single and (b) 10 randomly oriented double vacancies (at the same positions as the single vacancies) . Note the broadening due to intra-valley scattering present for single vacancy defects but absent for double vacancies (marked by black triangles).

and double vacancies lead to *inter*-valley scattering, only single vacancies cause a pronounced broadening of each peak [compare Fig. 4(a,b)]. This clearly demonstrates the strong *intra*-valley scattering due to single vacancies.

IV. SUBSTRATE INTERACTION

Apart from point defects in the graphene lattice, other sources of disorder in graphene nanodevices are substrate interactions or Coulomb charges. These lead to smooth correlated disorder potentials rather than to a point-like destruction of SU(2) symmetry. To elucidate the differences to point scatterers, we now include a random

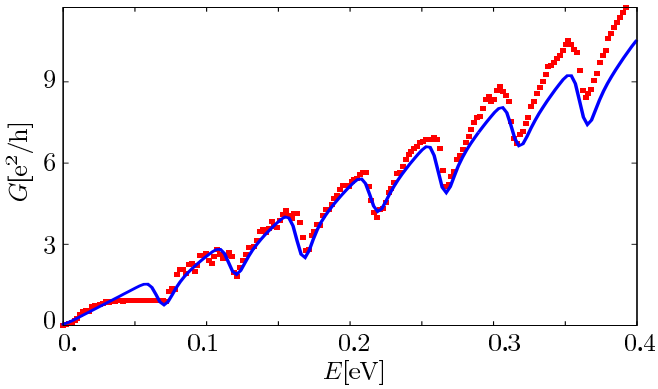

FIG. 5. Zero temperature conductance of a $W = 30nm$ wide ribbon as a function of energy for a disorder correlation length $\xi = 4nm$ and a disorder amplitude $V_0 = 100$meV. Dots represent quantum mechanical calculations, averaged over 100 disorder realizations. The blue line represents our model based on backscattering through evanescent modes [see Eq. (10)]. Deviations at higher energies can be attributed to deviations from a perfectly linear bandstructure (trigonal warping).

disorder potential with

$$\langle V(\mathbf{x}) \rangle = 0, \quad \langle V^2 \rangle = V_0^2 \tag{5}$$

and a correlation length ξ (the full-width half-maximum of the autocorrelation function) into the on-site energies of our Hamiltonian [see Eq. (1)]. For correlation lengths $\xi < 1nm$, of the order of the lattice unit cell and small compared to the electronic wavelength $\sim 2\pi/\delta k$, we find an approximately linear increase of transmission with energy [not shown], similar to the single-vacancy case (Fig. 3), for which the sublattice symmetry is broken as in the case for small ξ. For larger ξ in the range of $1nm < \xi < 10nm$, we find, however, a remarkably robust pattern with pronounced dips at the thresholds for the opening of new modes (see Fig. 5) which indicates the observability of size quantization effects albeit not of plateaus.

Similar dips have been reported in other numerical simulations[23] of disordered graphene nanoribbons. They have been attributed to peaks in the density of states (DOS) ρ of the infinite nanoribbon as new quasi-onedimensional channels open up. The scattering rate $\Gamma(E)$ from an incoming state $|nk\rangle$ to a final state $|n'k'\rangle$ as given by Fermi's golden rule,

$$\Gamma(E) \propto \sum_{n'} |\langle nk|H|n'k'\rangle|^2 \rho_{n'}(E)\,, \tag{6}$$

should be enhanced when the density of final states is large. This qualitative argument neither invokes specific properties of the transition matrix element nor the prevalence of backscattering. In the following we suggest a specific mechanism for backscattering. To elucidate the involved scattering process, we calculate the Fourier transform [Eq. (4)] as a function of energy (see Fig. 6).

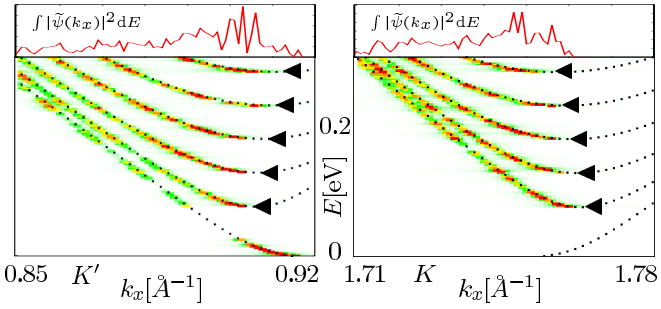

FIG. 6. Fourier transform $\mathcal{F}$ [see Eq. (4)] of the reflected wave as a function of energy for a 30nm wide zigzag nanoribbon (color indicates intensity of the reflected wave), containing a random disorder with amplitude $V_0 = 100meV$. The region around the K and K' cone are shown. The bandstructure [compare Fig. 2) is overlayed as black dots. The reflection is highest (see red color regions) near the opening of new modes (indicated by black triangles). This feature can also be identified in the energy integral of the reflected wave (see top row) which has its dominant contributions near the mode openings.

As incoming wave we choose a uniform superposition of all incoming modes. This choice assures a non-vanishing population amplitude of the entire discretized bandstructure near both the K and K' points. Accordingly, the reflected wave shows contributions from all modes. We observe that the major contribution to the dips in transmission originates from the highest mode open at E (see triangles and top inset in Fig. 6). This observation has immediate implications for the mode-dependence of the transition matrix element in (6). Key is the observation that the highest ($n = N$) available open mode may become locally evanescent when the smooth fluctuations of the disorder potential shift the band structure locally from a propagating to an evanescent mode. In turn, scattering into an evanescent mode strongly enhances backscattering as the memory on the original forward propagation direction is lost. Correspondingly, the opening of a new mode at a given energy E_N may not lead to a stepwise increase in transmission, but rather to a sharp decrease in the energy interval directly *above* E_N, when new scattering channels are about to become available. To give a quantitative estimate for this effect, we consider two contributions to transmission: a smooth background transmission,

$$T_0(E) \sim \frac{E}{\hbar v_{\rm F}} \frac{W}{\pi}, \tag{7}$$

originating from all propagating modes contributes a linear increase in the conductance ($\propto E$). Superposed on this smooth background is the contribution originating from scattering of locally evanescent modes. A mode with small (as compared to V_0) longitudinal energy

$$E_n^x = E - \hbar v_{\rm F} k_n \tag{8}$$

will become evanescent whenever the local disorder potential becomes larger than its remaining propagation energy E_n^x. For simplicity, we assume that the local value $V_{\rm loc}$ of the potential follows a uniform random distribution within the interval $[-V_0, V_0]$. The probability for a mode n to locally become evanescent (EV), which happens for $V_{\rm loc} > E_n^x$, is then given by

$$P_{{\rm EV},n} = \begin{cases} \frac{V_0 - E_n^x(E)}{2V_0}, & V_0 > E_n^x \\ 0, & V_0 < E_n^x \end{cases} \tag{9}$$

$P_{{\rm EV},n}$ is largest for the highest mode, $n = N$, and $E_N^x \to 0$, consistent with available numerical data showing that backscattering is largest right at the opening of a new mode (see Fig. 5).

We replace the transition matrix element, Eq. (6), for scattering into evanescent modes by Eq. (9), $|\langle nk|H|n'k'\rangle|^2 \sim P_{{\rm EV},n}$ with $(n'k')$ taken to be an evanescent mode. Accordingly, Fermi's golden rule for this specific backscattering process via evanescent modes becomes

$$R_{EV}(E) \propto P_{{\rm EV},N}(E)\rho_V(E)\,. \tag{10}$$

We have assumed here that reflection proceeds preferentially through scattering into the highest (evanescent) mode N. Furthermore we have replaced the DOS of the ideal ribbon ρ (featuring infinitely sharp peaks) by ρ_V, the DOS of the scattering geometry in the presence of the disorder potential V. As we have verified numerically, ρ_V can be approximated by averaging ρ over an energy window of about 15 meV. It is remarkable that Eq. (10) allows to quantitatively reproduce, up to a normalization constant, our numerical data very well [see blue line in Fig. 5]. In particular, $R_{EV}(E)$ captures the depth and shape of the transmission dips as a function of the relative strength of the potential V_0 compared to the energy distance between adjacent modes. Notice here the difference to the results obtained above for double vacancies which give rise to dips just below the quantization steps signifying scattering into "almost" open modes (see[24]). In contrast, for a smooth disorder potential the dips appear just *above* the quantization steps where the disorder potential can locally "close" an already open mode. The importance of the backscattering process via evanescent modes underlying Eq. (10) is plausible in view of the fact that, due to pseudospin conservation, smooth long-range disorder is less likely to directly backscatter forward propagating modes in graphene[20]. It would be interesting to substantiate the present results by a rigorous derivation including point defects and rough edges, following similar arguments as in, e.g.,[26], adapted to the zigzag nanoribbons considered here.

V. COMPARISON TO TRANSPORT EXPERIMENTS

We test our theoretical results by comparison with recent experimental data on the transmission through

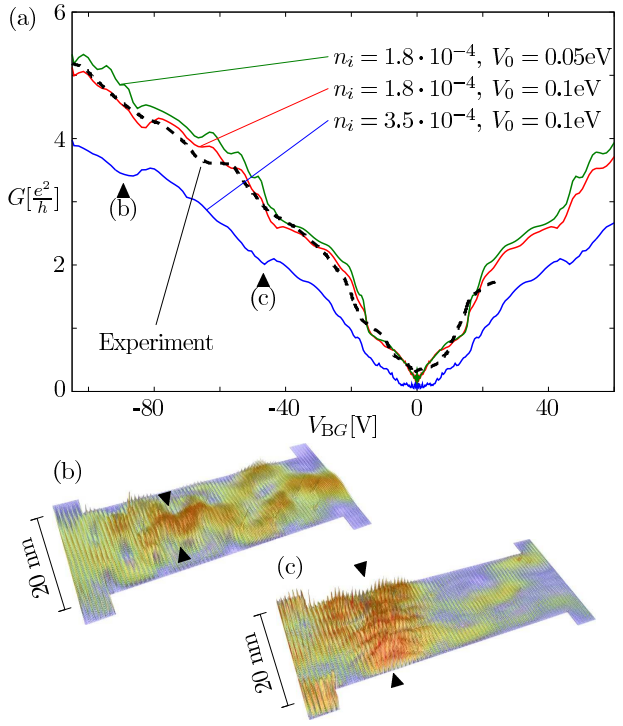

FIG. 7. (a) Conductance of a graphene nanoconstriction [dimensions see (b)] as function of back-gate voltage for three different combinations of single vacancies and correlated disorder (see insets, each curve corresponds to an average over 100 disorder configurations). Experimental data (black dashed line) taken from[6]. (b,c) Scattering states through the graphene junction, at energies marked by black triangles in (a). Black triangles in (b) and (c) mark pronounced enhancements of the wavefunctions.

graphene quantum nanoconstrictions[6,25]. For the theoretical description of large disordered graphene systems, phase-coherent tight-binding quantum transport calculations as well as semiclassical Boltzmann transport theory have been applied, for a review see[27]. However, recent results[28] suggest that standard Boltzmann-theory might not be well suited to correctly describe the difference between short-range and long-range scatterers in graphene. Conversely, a full quantum calculation in the quasi-ballistic regime should be able to distinguish between short range and long-range scatterers due to a different dependence of conductance on carrier density (and thus energy). We therefore aim to combine the effect of both short-range and long-range scatterers in one ballistic quantum-transport calculation. To avoid freely adjustable parameters, we take the disorder present from recent experiments. We infer a typical effective density of $K-K'$ scatterers from a measurement of the movement of Coulomb blockade peaks in a transverse magnetic field[29] indicating a defect density of approximately $n_i = 3.5 \times 10^{-4}$ effective single vacancy scatterers per carbon atom for a graphene dot on silicon dioxide substrate[29]. For the smoothly varying long-range disorder potential, we use an amplitude of $V_0 = 0.1$eV and a correlation length of $5nm$, as obtained from recent transport[30] and STM data[18] experiments for graphene on SiO_2. We include a wider contact region to incorporate reflection at the mouth of the nanoconstriction. The potential landscape of the constriction results in wave function enhancements inside the constriction [see solid triangles in Fig. 7(b,c)] causing transmission minima. We find good *qualitative* agreement between the measurement data [black dashed line in Fig. 7(a)] and our calculations, strongly hinting at short-range $K-K'$ scatterers and disorder playing a major role in the experiment. As suggested[28], short-range scatterers (i.e. impurity density n_i) and long-range disorder (averaged potential strength V_0) change the functional form of the conductance curve in different ways. Indeed, we can achieve *quantitative* agreement for a defect density of $n_i = 1.7 \times 10^{-4}$ [see red line in Fig. 7(a)], i.e., for fewer short-range scatterers than in the experiments on quantum dots[29]. We believe that the lower value for n_i, as compared to the value taken from experiments on quantum dots is related to the different circumference-to-area ratio of the nanoconstriction as compared to quantum dots. Since etched edges will contribute a sizable percentage of short-range scattering to an effective n_i, values for different geometries may vary. Additionally, for our particular geometry, results depend far more strongly on short-range scatterers than on the potential amplitude [see lines in Fig. 7(a)], hinting that, in this case, short range scattering (at, e.g., rough edges) seems the dominant source of scattering.

VI. CONCLUSIONS

We have investigated transport in bulk-disordered graphene nanoribbons and nanoconstrictions. Both point-like lattice defects and a correlated random disorder were studied. We find that for small correlation lengths (comparable to the lattice spacing), the disorder acts similar to a lattice vacancy, destroying size quantization. For longer correlation lengths $\xi > 1nm$, we observe strong dips as clear signatures of size quantization. We motivate the presence of these dips by a model based on Fermi's golden rule, yielding qualitative agreement with quantum transport simulations. To elucidate the role of inter-valley and intra-valley scattering we calculate the Fourier transformation of the scattered wave. Our results are compared to experimental data on transport through graphene nanoconstrictions.

We thank K. Ensslin, F. Guinea, J. Güttinger, and C. Stampfer for valuable discussions. Support by the Austrian Science Foundation and the FWF, SFB-041 (ViCoM) are gratefully acknowledged. Numerical Calculations where performed on the Vienna Scientific Cluster (VSC).

[1] K. S. Novoselov, A. K. Geim, S. V. Morozov, D. Jiang, M. I. Katsnelson, I. V. Grigorieva, S. V. Dubonos, and A. A. Firsov, Nature **438**, 197 (2005).

[2] Y. Zhang, Y. W. Tan, H. Stormer, and P. Kim, Nature **438**, 201 (2005).

[3] A. K. Geim and K. S. Novoselov, Nature Materials **6**, 183 (2007).

[4] B. Trauzettel, D. V. Bulaev, D. Loss, and G. Burkard, Nature Physics **3**, 192 (2007).

[5] M. V. Berry and R. J. Mondragon, Proc. R. Soc. Lond. A **412**, 53 (1987).

[6] L. A. Ponomarenko, F. Schedin, M. I. Katsnelson, R. Yang, E. H. Hill, K. S. Novoselov, and A. K. Geim, Science **320**, 356 (2008).

[7] H. Min, J. E. Hill, N. A. Sinitsyn, B. R. Sahu, L. Kleinman, and A. H. MacDonald., Phys. Rev. B **74**, 165310 (2006).

[8] N. Tombros, C. Jozsa, M. Popinciuc, H. T. Jonkman, and B. J. van Wees, Nature **448**, 571 (2007).

[9] N. Dombay and A. Calogeracos, Phys. Rep. **315**, 41 (1999).

[10] M. I. Katsnelson, K. S. Novoselov, and A. K. Geim, Nature Physics **2**, 620 (2006).

[11] N. Stander, B. Huard, and D. Goldhaber-Gordon, Phys. Rev. Lett. **102**, 026807 (2009).

[12] Z. Chen, Y. Lin, M. Rooks, and P. Avouris, Physica E **40**, 228 (2007).

[13] M. Y. Han, B. Özyilmaz, Y. Zhang, and P. Kim, Phys. Rev. Lett. **98**, 206805 (2007).

[14] Y. M. Lin, V. Perebeinos, Z. Chen, and P. Avouris, Phys. Rev. B **78**, 161409 (2008).

[15] F. Miao, S. Wijeratne, Y. Zhang, U. C. Coskun, W. Bao, and C. N. Lau., Science **317**, 1530 (2007).

[16] C. Stampfer, J. Güttinger, F. Molitor, D. Graf, T. Ihn, and K. Ensslin, Appl. Phys. Lett. **92**, 012102 (2008).

[17] C. Stampfer, E. Schurtenberger, F. Molitor, J. Güttinger, T. Ihn, and K. Ensslin, Nano Lett. **8**, 2378 (2008).

[18] V. Geringer, M. Liebmann, T. Echtermeyer, S. Runte, M. Schmidt, R. Rückamp, M. Lemme, and M. Morgenstern, Phys. Rev. Lett. **102**, 076102 (2009).

[19] S. Reich, J. Maultzsch, C. Thomsen, and P. Ordejón, Phys. Rev. B **66**, 035412 (2002).

[20] A. H. C. Neto, F. Guinea, N. M. R. Peres, K. S. Novoselov, and A. K. Geim, Rev. Mod. Phys. **81**, 109 (2009).

[21] E. R. Mucciolo, A. H. C. Neto, and C. H. Lewenkopf, Phys. Rev. B **79**, 075407 (2009).

[22] M. Evaldsson, I. V. Zozoulenko, H. Xu, and T. Heinzel, Phys. Rev. B **78**, 161407(R) (2008).

[23] S. Ihnatsenka, and G. Kirczenow, Phys. Rev. B **80**, 201407R (2009).

[24] F. Libisch, S. Rotter, and J. Burgdörfer, Suppression of size quantization in graphene nanoribbons, arXiv:1102.3848, (2011).

[25] N. Tombros, A. Veligura, J. Junesch, M. H. D. Guimaraes, I. J. V. Marun, H. T. Jonkman, and B. J. van Wees, Nature Physics **7**, 697 (2011).

[26] D. A. Areshkin, D. Gunlycke, and C. T. White, Nano Lett. **7**, 204 (2007).

[27] S. Das Sarma, S. Adam, E. H. Hwang, and E. Rossi, Rev. Mod. Phys. **83**, 407 (2011).

[28] J. W. Klos, and I. V. Zozoulenko, Phys. Rev. B **82**, 081414(R) (2008).

[29] F. Libisch, S. Rotter, J. Güttinger, C. Stampfer, and J. Burgdörfer, Phys. Rev. B **81**, 245411 (2010).

[30] C. Stampfer, J. Güttinger, S. Hellmüller, F. Molitor, K. Ensslin, and T. Ihn, Phys. Rev. Lett. **102**, 056403 (2009).